Comparison of plasma temperature and electron density on nanosecond laser ablation of Cu and nano-Cu

Anmin Chen, Yuanfei Jiang, Tingfeng Wang, Junfeng Shao, and Mingxing Jin

Citation: Physics of Plasmas **22**, 033301 (2015); doi: 10.1063/1.4913987
View online: http://dx.doi.org/10.1063/1.4913987
View Table of Contents: http://scitation.aip.org/content/aip/journal/pop/22/3?ver=pdfcov
Published by the AIP Publishing

Comparison of plasma temperature and electron density on nanosecond laser ablation of Cu and nano-Cu

Anmin Chen,[1,2] Yuanfei Jiang,[1,2] Tingfeng Wang,[3] Junfeng Shao,[3] and Mingxing Jin[1,2,3,a)]
[1]*Institute of Atomic and Molecular Physics, Jilin University, Changchun 130012, China*
[2]*Jilin Provincial Key Laboratory of Applied Atomic and Molecular Spectroscopy (Jilin University), Changchun 130012, China*
[3]*State Key Laboratory of Laser Interaction with Matter, Changchun Institute of Optics, Fine Mechanics and Physics, Chinese Academy of Sciences, Changchun 130033, China*

(Received 19 September 2014; accepted 19 February 2015; published online 3 March 2015)

Laser-induced breakdown spectroscopy is performed through the collection of spectra by spectral detection equipment at different delay times and distances from targets composed of Cu and nano-Cu, which are ablated using a Nd:YAG laser (532 nm, 10 ns, 10 Hz) in our experiments. The measured wavelength range is from 475 nm to 525 nm. Using the local thermodynamic equilibrium model, we analyze the characteristics of the plasma temperature and the electron number density for different distances between the target surface and the lens. The results show that when compared with the nano-Cu plasma case, the temperature of the Cu plasma is higher, while its electron number density is lower. © *2015 AIP Publishing LLC*.
[http://dx.doi.org/10.1063/1.4913987]

I. INTRODUCTION

Since the invention of the laser in 1960, laser-induced breakdown spectroscopy (LIBS) has attracted increasing research attention.[1] LIBS is performed by focusing the laser on a small area at the surface of the specimen of interest, which is then ablated on a scale ranging from nanograms to picograms, and a plasma plume can be generated. In principle, LIBS can be used to analyze any matter, regardless of its physical state, whether it is solid, liquid, or gaseous.[2,3] Because all elements emit light with characteristic frequencies when excited to high temperatures, all of them can be detected by LIBS, which is only limited by the power of the laser, and the sensitivity and wavelength range of the spectrograph and the detector.

Many reports have indicated that LIBS may be varied by adjustment of the laser parameters, including the laser wavelength, pulse width, and intensity.[4–7] The properties of LIBS also depend on the laser spot size, and on the distance between the target and the lens. The sample position has an important influence on the plasma plume expansion process because of the interaction between the plasma plume and the laser spatial energy distribution.[4,8,9] In recent years, several new experimental methods have been used to improve the sensitivity of LIBS, including plasma confinement,[10,11] fast spark discharge,[12] magnetic fields,[13] and double pulse methods.[14,15] In particular, Giacomo *et al.*[16] studied nanoparticle-enhanced LIBS of metallic samples in 2014. In this work, LIBS was found to be strongly enhanced if the nanoparticles that were deposited on the metal surface were used to lower the breakdown threshold. This is because the nanoparticles can significantly increase the laser-matter interaction. Therefore, research into laser ablation using metal nanoparticles is of considerable importance to the understanding of nanoparticle-enhanced LIBS.

The motivation of this work is to enhance our understanding of the mechanism of laser–matter interaction. In this paper, targets composed of Cu and nano-Cu are ablated by nanosecond laser pulses. The differences between the plasma spectroscopy characteristics of Cu and nano-Cu are then investigated using optical emission spectroscopy. The plasma parameters studied by this paper (e.g., plasma temperature and electron density) could provide enhanced understanding of many plasma processes. We investigate the plasma temperature and the electron number density on nanosecond laser ablation of the Cu and nano-Cu targets, and compare the results.

II. EXPERIMENTAL SETUP

The apparatus used is shown schematically in Fig. 1. The laser system is a Q-switched Nd:YAG laser (Spectra Physics, Quanta-Ray DCR-2A). The full-width at half maximum (FWHM) of the pulse is 10 ns, the maximum output energy is approximately 80 mJ, the wavelength is 532 nm, which is generated using the second harmonic wavelength from the fundamental wavelength of 1064 nm, and the repetition rate is 10 Hz. Plasma spectroscopy is performed by focusing the laser pulses on the targets in a vacuum. The pressure of the vacuum chamber is 4×10^{-2} Torr. The target is mounted on a rotating stepper stage, which guarantees that the sample location used is renewed before each laser shot. The sample is located at an angle of 45° with respect to the direction of the laser beam. The emission spectra are focused on a fiber using two lenses, which are orientated parallel to the target surface. The imaging ratio is 1.26:1. The fiber tip is positioned using another stepper stage. This stage is oriented perpendicular to the target surface. The spatial spectra can then be detected, and the spectra are guided to a

a)Author to whom correspondence should be addressed. Electronic mail: mxjin@jlu.edu.cn

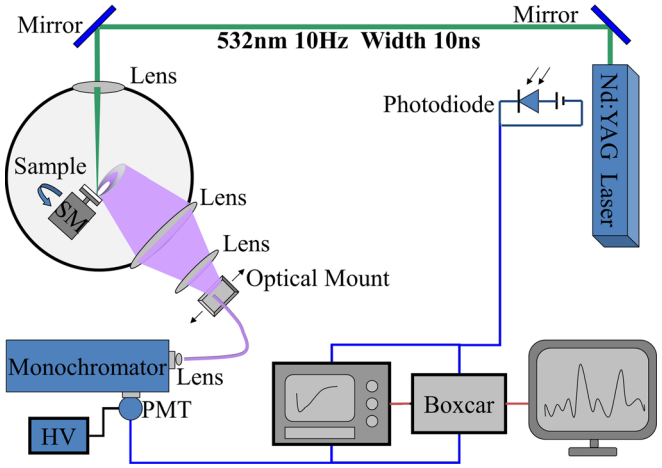

FIG. 1. Experimental setup for spectroscopy measurement of nanosecond laser ablation Cu and NanoCu.

monochromator (WDG500–1A) through the fiber. The slit size is 0.5 μm. The grating used in the experiments has 1200 grooves/mm. The spectral intensity is detected using a photomultiplier tube (PMT, CR114) with a voltage range of 900 V–1200 V. The electrical signal generated by the light intensity signal is sent to Boxcar SR250. The signal is then converted into a digital signal by Boxcar SR245. The final measured data are recorded by a computer. A photodiode receives an optical signal to trigger the Boxcar, which guarantees time synchronization of the laser signal and the spectral signal. An oscilloscope (Lecroy9361) displays the delay times of the two signals. A low-pressure Hg lamp is used for wavelength calibration.

One of the samples is bulk Cu with the purity of 99.9%. Another sample is nano-Cu block. In this nano-Cu block, the copper nanoparticles are prepared by flow-levitation method.[18] The produced copper nanoparticles are mechanically compacted for 40 min under pressure of 1.5 GPa by cold pressing method. The pressing process is carried out well under 25 °C and inert gas protection. The surface of nano-Cu block is smooth with the purple. From the XRD spectrum, the nano-Cu is the face-centered cubic structure. By the warren Averbach method of peak shape analysis, the average grain size of nanoparticles in nano-Cu is 22.8 nm, micro strain is 0.073%. However, for nano-Cu powder, the average grain size of nanoparticles is 22.6 nm, micro strain is 0.039%. This shows that the effect of pressure on the nano-Cu grain size is small, the micro strain increases from 0.039% to 0.073%. The relative density of nano-Cu block is about 94%, micro hardness is about 2.0 GPa.

III. RESULTS AND DISCUSSION

In laser ablation, the absorption mechanism for metals is the inverse bremsstrahlung (IB) absorption process. For nanosecond laser ablation of metals, the principal mechanisms of material removal are vaporization and phase explosion.[19] These phenomena are thermal, because the duration of the nanosecond laser pulse is greater than the electron–phonon relaxation time of the metal.[20] Figure 2 compares the spectral intensity of laser ablation of (a) Cu and (b)

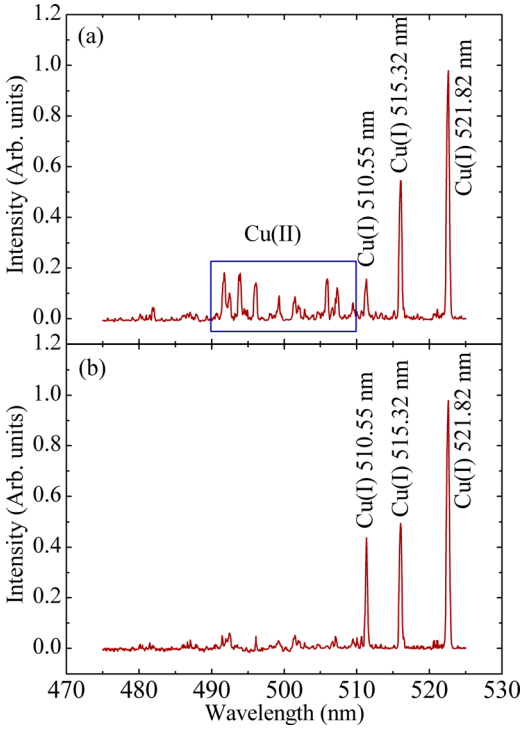

FIG. 2. Spectral intensity at the range from 475 nm to 525 nm for laser ablation (a) Cu and (b) NanoCu. The energy is 40 mJ, the delay time is 1000 ns, the integral time is 30 ns, the pressure is 0.04 Torr, and the distance of target surface is 5.04 mm, respectively.

nano-Cu over the range from 475 nm to 525 nm. The pulse energy is 40 mJ, the delay time is 1000 ns, the integral time is 30 ns, the operating pressure is 0.04 Torr, and the distance to the target surface is 5.04 mm. The Cu plasma emission spectrum mainly consists of Cu (I) and Cu (II) lines. For laser ablation of nano-Cu, the emission lines are composed of Cu (I) lines only; almost no Cu (II) spectral lines were observed. The plasma spectra results reported by Kumar and Thareja[21] in different environments are similar to the experimental results reported here for the spectra of Cu and nano-Cu. The Cu transitions that were observed for Cu and nano-Cu are Cu (I) $(3d^{10}4p^1(^2P_{3/2}) - 3d^9 4s^2(^2D_{5/2})$ at 510.5 nm), Cu (I) $(3d^{10}4d^1(^2D_{3/2}) - 3d^{10}4p^1(^2P_{1/2})$ at 515.3 nm), and Cu (I) $(3d^{10}4d^1(^2D_{3/2}) - 3d^{10}4p^1(^2P_{3/2})$ at 521.8 nm).

The nano-Cu target consists of nanoparticles and the resulting plasma will include many more nanoparticles than the Cu case. During nanosecond laser irradiation, based on thermionic emission, the nanoparticle surface will absorb the laser energy to generate electron emission, and collisions among the particles also can produce more electrons. These two processes will consume a great deal of energy. When compared with the bulk Cu, the electron density is high and the temperature is low for nano-Cu. For bulk Cu, in the plasma produced by ns laser irradiation of the Cu target, the number of atoms is larger than that of the nano-Cu plasma, and the energy consumption by the thermionic emission or collision processes is less than in the nano-Cu case. The plasma temperature can be increased to a high temperature regime, and then the atoms will be ionized. This enables the Cu (II) lines to be observed. The plasma is not heated to a

sufficiently high temperature for Cu (III) lines to be observed.

The plasma spectra are analyzed using LS coupling rules and the NIST atomic spectra database.[22] The plasma excitation temperature is determined using the Boltzmann plot method by assuming that the plasma is in local thermodynamic equilibrium (LTE) and is optically thin.[17] The excitation temperature is determined using the following equation:[23–25]

$$\ln\left(\frac{\lambda_{ij}I_{ij}}{g_iA_{ij}}\right) = -\frac{E_i}{k_BT_e} + C, \tag{1}$$

where I_{ij}, λ_{ij}, and A_{ij} are the intensity, the wavelength, and the transition probability, respectively. g_i is the statistical weight of the upper level. E_i is the energy of the upper state. k_B and T_e are the Boltzmann constant and the excitation temperature, respectively. By plotting the left-hand side $(\ln(I\lambda/gA))$ of (1) versus the excited-level energy term E_i, the excitation temperature is calculated from the slope of the straight line obtained $(-1/k_BT)$.The plasma temperature can be determined without knowledge of the total number density or the partition function.[26]

The lines of Cu (I) $(3d^{10}4p^1(^2P_{3/2}) - 3d^94s^2(^2D_{5/2})$ at 510.5 nm), Cu (I) $(3d^{10}4d^1(^2D_{3/2}) - 3d^{10}4p^1(^2P_{1/2})$ at 515.3 nm), and Cu (I) $(3d^{10}4d^1(^2D_{3/2}) - 3d^{10}4p^1(^2P_{3/2})$ at 521.8 nm) are used to calculate the plasma excitation temperature (T_e). The spectroscopic details of the transition lines are listed in Table I. An example of the Boltzmann plots is shown in Fig. 3 using the selected lines. In fact, to reduce the data errors, more data points from the upper energy levels should be used to fit a straight line. Fewer data points lead to larger errors.

The spatial variation of the plasma temperature at different delay times is presented in Fig. 4. The laser pulse energy is 40 mJ. The process pressure is 4×10^{-2} Torr. The solid lines are intended as a guide to the eye only. When the target distance is greater than 5 mm for the Cu plasma, it is difficult to estimate the plasma temperature based on the plasma spectrum produced because the emission intensity is very weak. For Cu and nano-Cu, the plasma excitation temperature close to the surface of the target is low, and the temperature increases with increasing distance up to 5.0 mm from the target surface, which is caused by rapid plasma expansion and a high strong collision frequency;[27–29] at a distance of 5.0 mm from the target surface, the rate of plasma cooling is low due to strong collisions caused by the shockwave effect.[30,31] Figure 5 shows the evolution of the plasma temperature as produced by laser ablation of Cu and nano-Cu as a function of the delay time. The distance to the target surface is 1.26 mm. As the delay time increases, the corresponding excitation temperature decreases because the thermal energy is rapidly converted into kinetic energy when the plasma attains a high expansion velocity, leading to a decline in the temperature of the expanding plasma.[25] As shown in Figs. 4 and 5, the plasma temperature for nano-Cu is lower than that of laser-ablated Cu, although the total energy of the laser pulses is the same, because the breakdown threshold of the metallic nanoparticles is much lower than that of the bulk metal.[16] When compared with the plasma of the bulk Cu, the nano-Cu plasma produced by the laser pulses can obtain a higher expansion velocity. Therefore, in the nano-Cu case, the plasma temperature is low and the expansion distance is long.

TABLE I. Spectroscopic parameters of Cu (I) transition lines used to calculate excitation temperature.[22]

Wavelength (nm)	$E_i(\text{cm}^{-1})$	$E_j(\text{cm}^{-1})$	g_i	g_j	$A_{ij}(\times 10^8\text{s}^{-1})$
510.55	30783.69	11202.56	4	6	0.020(5)
515.32	49935.2	30535.3	4	2	0.60(15)
521.82	49942.06	30783.69	6	4	0.75(9)

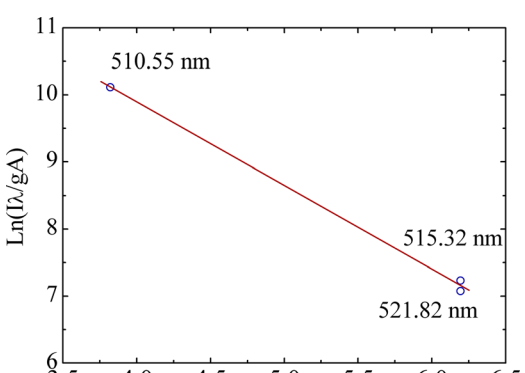

FIG. 3. Examples of Boltzmann plots of Cu plasma spectroscopy from Fig. 2. The calculated excitation temperature is 0.9×10^4 K.

The FWHM of each line can be used to determine the electron number density.[26,32,33] In the experiments, the electron number density is determined from the line profile of an isolated Cu neutral line at 521.83 nm by neglecting the contributions of ion impact broadening and Doppler broadening as follows:[34–36]

$$\Delta\lambda_{1/2} = 2\omega\left(\frac{N_e}{10^{16}}\right), \tag{2}$$

where N_e is the electron number density. The value of ω that corresponds to the Cu-neutral line at 521.83 nm was obtained from published data.[37]

Figure 6 shows the electron number density distribution with axial distance from the target surface. The spectral line is fitted using a Voigt profile. The delay times used are 300 ns and 500 ns. Because of an increase in the recombination rates for the ionic species in the 0 mm–2.5 mm range from the target surface, the electron number density decreases rapidly within this region for 300 ns (Fig. 6(a)). For the delay time of 500 ns (Fig. 6(b)), the electron number density variation with axial distance is slow, in the range from 0 mm to 4 mm, because the plasma undergoes expansion into a large-volume plume. The electron number density is plotted as a function of the delay time in Fig. 7. The distance to the target surface is 1.26 mm. The evolution of the function indicates that the electron number density is highest at the initial stage of the plasma and then decreases with increasing delay time. In the range from 800 ns to 1200 ns,

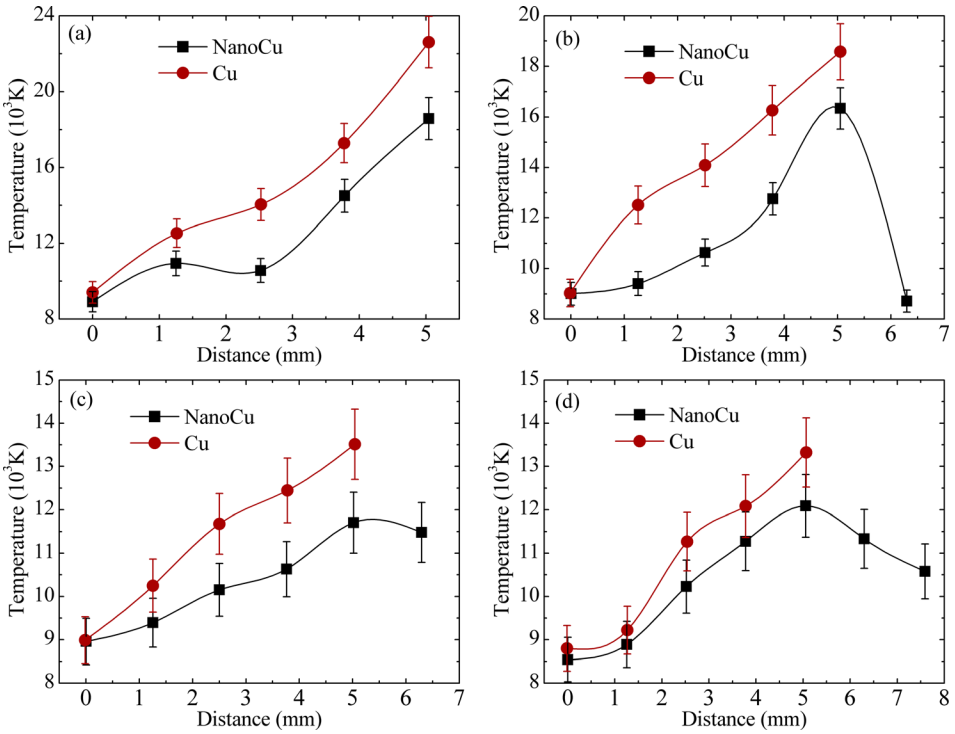

FIG. 4. Variation of excitation temperature produced by laser ablation Cu and NanoCu along the distance from target surface. The delay time is 300 ns (a), 500 ns (b), 800 ns (c), and 1200 ns (d), respectively. The laser energy is 40 mJ. The pressure is 4×10^{-2} Torr.

the electron number density decay rate of the nano-Cu plasma is lower than that of the Cu plasma. The interaction between the laser and the nano-Cu target leads to stronger collisions between the particles (electrons, ions, atoms, and nanoparticles) in the plume of the plasma, which results in the electron number density decay time being significantly prolonged.

In the target laser irradiation process, according to classical electromagnetic theory,[38] when the laser energy is absorbed at the light penetration depth of the target, the plasma will be produced and the plasma excitation temperature will increase.[39] However, during the interaction of the laser beam with the nanoparticles, more laser energy can be transmitted through the interior of the target. This is equivalent to an increase in the light penetration depth of the target. The laser energy can then be deposited in the interior of the target, and we deduce that more of the target material can be removed for laser ablation of nano-Cu, which causes the plasma plume created by the laser pulse to expand and become much larger. Also, the collisions among the electrons, atoms, ions, and the increased number of nanoparticles (where the target consists of these nanoparticles) in the plasma generate more electrons, and this is the direct cause of the relatively high electron number density when

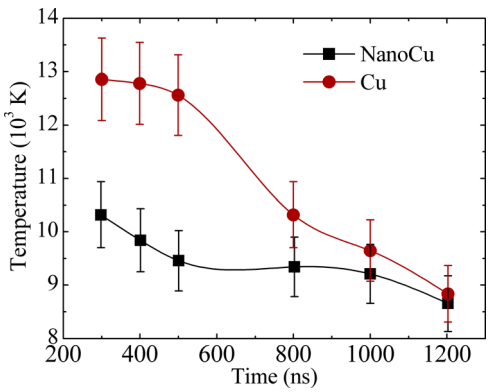

FIG. 5. Variation of excitation temperature produced by laser ablation Cu and NanoCu with the delay time. The distance from target surface is 1.26 mm. The laser energy is 40 mJ. The pressure is 4×10^{-2} Torr.

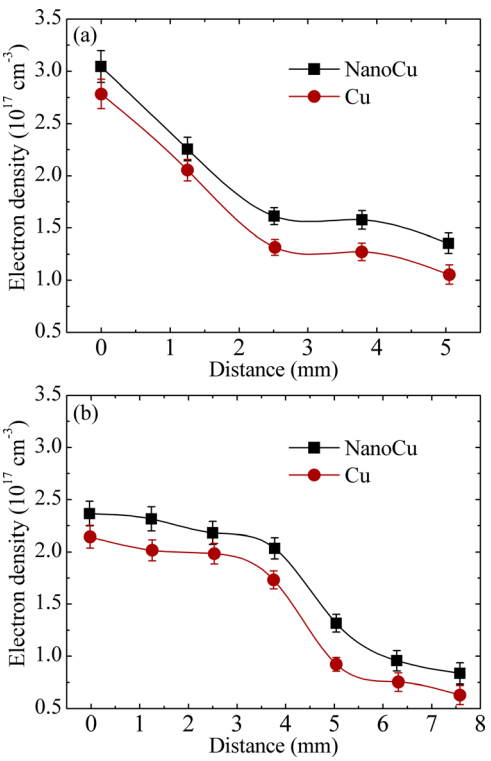

FIG. 6. Variation of electron density produced by laser ablation Cu and NanoCu along the distance from target surface. The delay time is 300 ns (a), and 500 ns (b). The laser energy is 40 mJ. The pressure is 4×10^{-2} Torr.

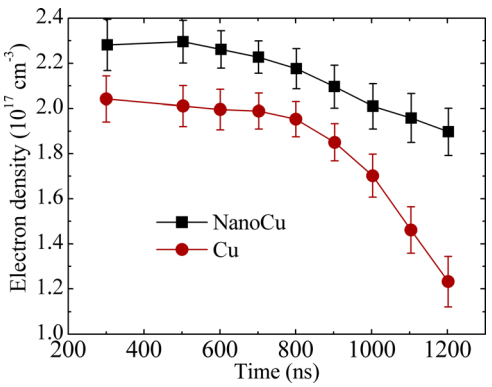

FIG. 7. Variation of electron density produced by laser ablation Cu and NanoCu with the delay time. The distance from target surface is 1.26 mm. The laser energy is 40 mJ. The pressure is 4×10^{-2} Torr.

compared with that of bulk Cu. These extra electrons need more energy, which causes the excitation temperature to be lower than that of bulk Cu plasma.

Unlike the nano-Cu case, the light cannot penetrate any deeper into the target during laser ablation of bulk Cu and concentrates at the target surface, which means that the plasma temperature is higher. However, while the temperature of the plasma produced by the laser pulse has become relatively high, the electron number density of the Cu plasma is lower than that of the nano-Cu plasma. It is obvious that there are fewer nanoparticles in the Cu plasma than in the nano-Cu plasma, and the collisions in the Cu plasma are weaker than those in the nano-Cu plasma. Accordingly, the number of electrons generated by the collision is also lower. We can therefore understand the mechanism of laser ablation of nanoparticles from the differences in plasma temperature and electron density between the Cu and nano-Cu plasmas.

IV. CONCLUSION

This work is focused on investigation of nanosecond laser ablation of bulk Cu and nano-Cu. The temporally and spatially resolved plasma spectra are collected by the spectral detection system in a wavelength range from 475 nm to 525 nm. For laser ablation of nano-Cu, only Cu (I) lines and almost no Cu (II) spectral lines are observed. Using the local thermodynamic equilibrium model, we analyzed the plasma temperature and electron density characteristics near the target. The results show that the plasma temperature of the Cu plasma is higher than that of the nano-Cu plasma, while the electron number density of the Cu plasma is lower than that of the NanoCu plasma. Therefore, we have been able to understand the mechanism of laser ablation of nanoparticles from the differences in plasma temperature and electron number density between the Cu and nano-Cu plasmas.

ACKNOWLEDGMENTS

We thank Dr. Jing Guo for her help in English. This project was supported by the National Basic Research Program of China (973 Program, Grant No. 2013CB922200), the China Postdoctoral Science Foundation (Grant No. 2014M551169), the Fundamental Research Funds for the Central Universities, and the National Natural Science Foundation of China (Grant Nos. 10974069 and 11034003).

[1]A. W. Miziolek, V. Palleschi, and I. Schechter, *Laser-Induced Breakdown Spectroscopy (LIBS)* (Cambridge University Press, Cambridge, 2006).
[2]F. J. Fortes, J. Moros, P. Lucena, L. M. Cabalin, and J. J. Laserna, Anal. Chem. **85**, 640 (2013).
[3]O. T. Butler, W. R. L. Cairns, J. M. Cook, and C. M. Davidson, J. Anal. At. Spectrom. **29**, 17 (2014).
[4]S. S. Harilal, J. Appl. Phys. **102**, 123306 (2007).
[5]S. S. Harilal, R. W. Coons, P. Hough, and A. Hassanein, Appl. Phys. Lett. **95**, 221501 (2009).
[6]J. T. Schiffem, D. W. Doerr, and D. R. Alexander, Spectrochim. Acta Part B **62**, 1412 (2007).
[7]Y. Lu, V. Zorba, X. L. Mao, R. E. Zheng, and R. E. Russo, J. Anal. At. Spectrom. **28**, 743 (2013).
[8]A. Kasperczuk, T. Pisarczyk, M. Kalal, J. Ullschmied, E. Krousky, K. Masek, M. Pfeifer, K. Rohlena, J. Skala, and P. Pisarczyk, Appl. Phys. Lett. **94**, 081501 (2009).
[9]H. Qi, L. Suyu, Y. Qi, A. Chen, Z. Hu, X. Huang, J. Mingxing, and D. Ding, J. Anal. At. Spectrom. **29**, 1105 (2014).
[10]Z. Y. Hou, Z. Wang, J. M. Liu, W. D. Ni, and Z. Li, Opt. Express **21**, 15974 (2013).
[11]A. M. Popov, F. Colao, and R. Fantoni, J. Anal. At. Spectrom. **25**, 837 (2010).
[12]W. D. Zhou, X. J. Su, H. G. Qian, K. X. Li, X. F. Li, Y. L. Yu, and Z. J. Ren, J. Anal. At. Spectrom. **28**, 702 (2013).
[13]P. K. Pandey and R. K. Thareja, Phys. Plasmas **20**, 022117 (2013).
[14]A. Chen, S. Li, S. Li, Y. Jiang, J. Shao, T. Wang, X. Huang, M. Jin, and D. Ding, Phys. Plasmas **20**, 103110 (2013).
[15]J. Guo, T. Wang, J. Shao, T. Sun, R. Wang, A. Chen, Z. Hu, M. Jin, and D. Ding, Opt. Commun. **285**, 1895 (2012).
[16]A. De Giacomo, R. Gaudiuso, C. Koral, M. Dell'Aglio, and O. De Pascale, Anal. Chem. **85**, 10180 (2013).
[17]A. Montaser and D. Golightly, *Inductively Coupled Plasmas in Analytical Atomic Spectrometry* (VCH, New York, 1987).
[18]C. M. Li, H. Lei, Y. J. Tang, J. S. Luo, W. Liu, and Z. M. Chen, Nanotechnology **15**, 1866 (2004).
[19]A. Miotello and R. Kelly, Appl. Phys. Lett. **67**, 3535 (1995).
[20]A. H. A. Lutey, J. Appl. Phys. **114**, 083108 (2013).
[21]B. Kumar and R. K. Thareja, Phys. Plasmas **20**, 053503 (2013).
[22]See http://physics.nist.gov/PhysRefData/ASD/lines_form.html for NIST Atomic Spectra Database.
[23]M. S. Dawood and J. Margot, AIP Adv. **4**, 037111 (2014).
[24]Y. Li, H. Z. Zhang, Z. K. Jiang, Z. S. Li, and C. H. Hu, Optik **125**, 2851 (2014).
[25]M. Hanif, M. Salik, and M. A. Baig, Opt. Lasers Eng. **49**, 1456 (2011).
[26]H. Hegazy, E. AlAshkar, H. H. Abou-Gabal, M. N. Aly, and N. Hamed, IEEE Trans. Plasma Sci. **42**, 1674 (2014).
[27]S. George, A. Kumar, R. K. Singh, and V. P. N. Nampoori, Appl. Phys. Lett. **94**, 141501 (2009).
[28]S. S. Harilal, C. V. Bindhu, M. S. Tillack, F. Najmabadi, and A. C. Gaeris, J. Phys. D: Appl. Phys. **35**, 2935 (2002).
[29]X. W. Li, W. F. Wei, J. Wu, S. L. Jia, and A. C. Qiu, J. Phys. D: Appl. Phys. **46**, 475207 (2013).
[30]S. S. Harilal, G. V. Miloshevsky, P. K. Diwakar, N. L. LaHaye, and A. Hassanein, Phys. Plasmas **19**, 083504 (2012).
[31]S. Mahmood, R. S. Rawat, S. V. Springham, T. L. Tan, and P. Lee, Appl. Phys. A Mater. Sci. Process. **101**, 701 (2010).
[32]X. Zeng, X. Mao, S. S. Mao, J. H. Yoo, R. Greif, and R. E. Russo, J. Appl. Phys. **95**, 816 (2004).
[33]G. Shukla and A. Khare, Appl. Surf. Sci. **255**, 8730 (2009).
[34]H. Hegazy, F. M. Abdel-Rahim, and S. H. Allam, Appl. Phys. B: Lasers Opt. **108**, 665 (2012).
[35]M. A. Khater, Appl. Surf. Sci. **286**, 156 (2013).
[36]N. M. Shaikh, S. Hafeez, M. A. Kalyar, R. Ali, and M. A. Baig, J. Appl. Phys. **104**, 103108 (2008).
[37]M. A. Hafez, M. A. Khedr, F. F. Elaksher, and Y. E. Gamal, Plasma Sources Sci. Technol. **12**, 185 (2003).
[38]G. Bekefi and W. P. Allis, *Principles of Laser Plasmas* (Wiley, New York, 1976).
[39]H. Hegazy, H. A. Abd El-Ghany, S. H. Allam, and T. M. El-Sherbini, Appl. Phys. B: Lasers Opt. **110**, 509 (2013).